Rapid Local Changes in Helicity and Vertical Wind Shear Associated with the Passage of Ducted Gravity Waves

DRAFT, SUBMITTED

TIMOTHY A. COLEMAN AND KEVIN R. KNUPP

Department of Atmospheric Science, The University of Alabama in Huntsville

Submitted to Weather and Forecasting November 2007

Ducted gravity waves are associated with potentially large perturbations in horizontal winds. It may be shown, neglecting friction, that these perturbations are maximized at the surface and minimized at the top of the wave duct, producing perturbation vertical wind shear as well. The magnitude of this shear is maximized in the wave ridge and the wave trough. The perturbation shear may be significant, on the order of 10^{-2} s^{-1}. It is also shown that the perturbation vertical shear associated with the passage of a ducted gravity wave may significantly increase or decrease the storm-relative helicity over 30-60 minute time periods in the environment of a supercell storm. This could result in a source of transient horizontal vorticity which may be tilted into the vertical by a storm updraft.

1. Introduction

The surface wind perturbations associated with the passage of gravity waves were noted early on (e.g., Brunk 1949; Freeman 1948). The wave impedance relationship (Gossard and Munk 1954; Gossard and Hooke 1975) shows that the perturbations of wind and pressure associated with gravity waves are correlated with one another. The simple model of an atmospheric wave developed by Eom (1975), and illustrated by Bosart and Sanders (1986), shows that the wind perturbations of largest magnitude occur at lower levels of the atmosphere. This implies that there is perturbation vertical shear associated with the wind perturbations in an atmospheric gravity wave.

This perturbation vertical shear becomes important when gravity waves are present in a thunderstorm environment. Storm structure and intensity has been shown to be related to wind shear (e.g., Weisman and Klemp 1982, 1984), and many authors (e.g., Rotunno and Klemp 1982, 1985; Klemp 1987; Houze 1993) have examined the ways in which the interaction between the updraft and vertical shear produce dynamic pressure perturbations which may enhance the updraft on a given flank and affect storm motion. More significantly, Davies-Jones et al. (1990) showed that storm-relative helicity, a quantity related to the storm inflow and the vertical wind shear in the storm environment, is related to storm rotation. The perturbation vertical shear associated with a gravity wave may also affect the storm-relative helicity.

The changes in storm-relative helicity associated with a gravity wave passage may be significant. Miller and Sanders (1980) observed that tornadogenesis was increased when thunderstorm clusters interacted with gravity wave packets during the Super Outbreak of 3-4 April 1974. Others have observed changes in storm rotation associated with the storm's interaction with a gravity wave (e.g., Kilduff 1999). Simple numerical simulations have shown that the intensity of a pre-existing mesocyclone may change upon interaction with

a gravity wave (Coleman and Knupp 2006). More recently, Markowski and Richardson (2007) demonstrated large spatial variability in vertical shear and storm-relative helicity associated with mesoscale boundaries and convective rolls, and in one case the variability may have been associated with gravity waves.

In this paper, we intend to demonstrate the sudden and large impact a ducted gravity wave may have on the vertical wind shear and storm-relative helicity at a given location. This impact will be demonstrated both theoretically, using a basic numerical model for a ducted gravity wave, and with observations. In section 2, the kinematics of ducted gravity waves are reviewed. Section 3 examines idealized examples of gravity waves in an atmosphere with linear background shear, and how these waves affect the vertical shear and storm-relative helicity. Case studies are presented in section 4, and section 5 contains conclusions.

2. Ducted Gravity Waves

a. Basic Kinematics

A ducted gravity wave is, essentially, the superposition of two internal gravity waves, one propagating upward and one propagating downward. The downward waves are reflected upward by the ground. The upward waves are reflected by an atmospheric layer characterized by a vertical gradient in the Scorer parameter l (Scorer 1949). The Scorer parameter l is related to the static stability (given by the Brunt-Vaisala frequency N) and the vertical gradient in vertical wind shear (e.g., Lindzen and Tung 1976; Jin et al. 1996).

It may be shown (Lindzen and Tung 1976) that when the height of the reflecting level is ¼ of a vertical wavelength of the internal waves, the upward- and downward- propagating waves constructively interfere. In such a case, the atmospheric layer between the ground and the reflecting level is known as a "wave duct".

Mathematically, the horizontal wind perturbation in the direction of wave motion (u') associated with a two-dimensional internal gravity wave in the x-z plane is given by A cos ($kx + mz - \omega t$), where k is the horizontal wavenumber, m is the vertical wavenumber, and ω is the angular frequency. (It should be noted that the x-direction is taken to be the direction of wave motion.) The sign of the mz term determines the direction of propagation in the vertical.

Since a ducted wave is the superposition of an upward- and downward-propagating wave, the horizontal wind perturbation associated with a ducted gravity wave may be written as

$$u' = \mathrm{B} \cos (kx - \omega t) \cos (mz), \qquad (1)$$

where B = 2A. This implies that the maximum horizontal wind perturbations are at the surface (z=0), decreasing to u'=0 at the top of the duct (where $mz = \pi/2$). At any given z, u' exhibits a sinusoidal variation in x and t. The airflow in the x-z plane of a ducted gravity wave with horizontal wavelength 100 km, duct depth 2 km, and B = 10 m s^{-1} is shown in Figure 1.

The linear wave impedance relationship (e.g., Gossard and Munk 1954; Gossard and Hooke 1975) states that $u' = p' \rho^{-1} (c\text{–U})^{-1}$, where p' is the pressure perturbation, c is the ground-relative phase speed of the wave, U is the component of the background wind normal to wave motion, and c-U is the intrinsic wave phase speed. This implies that p' and u' are correlated. So, in the ducted wave example illustrated in Fig. 1, the maximum p' (the wave ridge) occurs at x = 0 km and x = 100 km, while the minimum p' (the wave trough) occurs at x = 50 km. Such a correlation between p' and u' has been noted by many authors (e.g., Trexler and Koch 2000; Bosart and Sanders 1986).

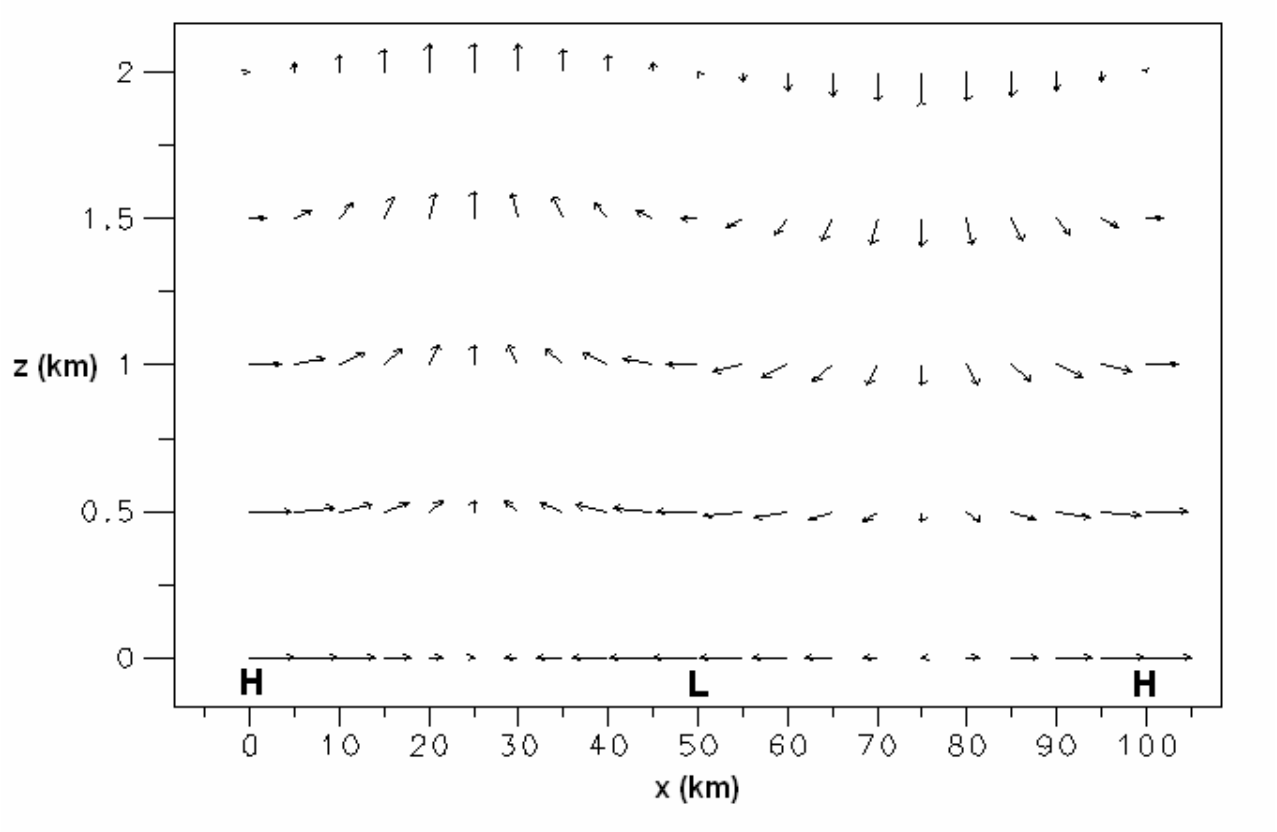

Figure 1. Perturbation airflow vectors in the *x*-*z* plane of a ducted gravity wave. The wave ridges are denoted by **H** and the wave trough is denoted by **L**.

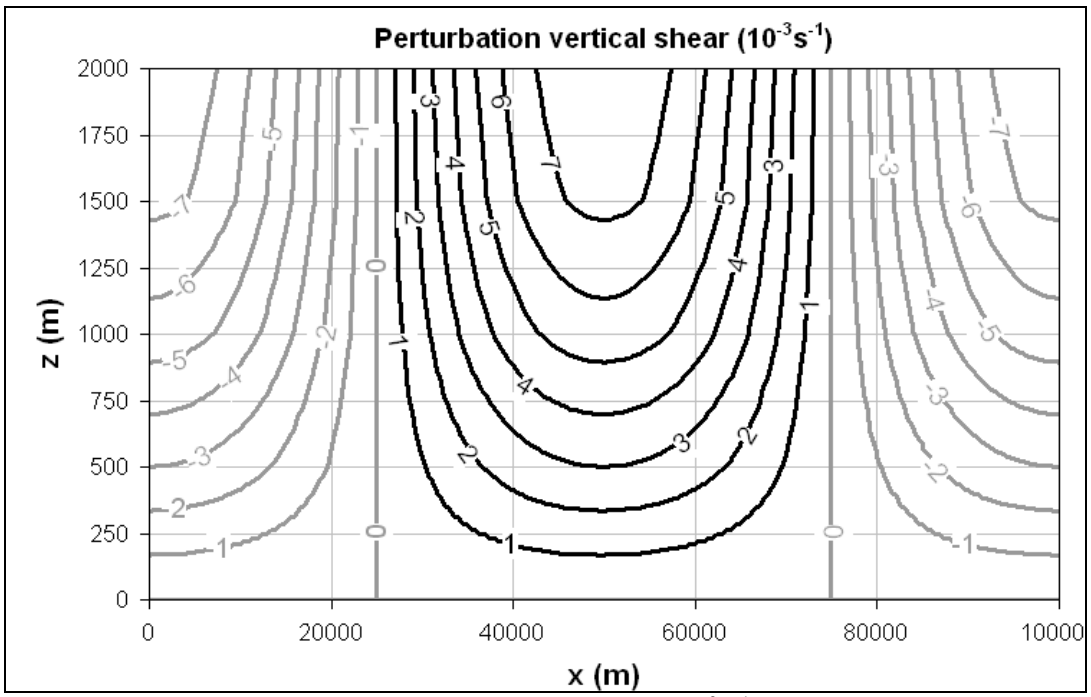

Figure 2. Magnitude of the perturbation vertical shear $\partial u'/\partial z$ (10^{-3} s^{-1}) associated with the ducted gravity wave in Fig. 1. Negative shear values are shaded in gray.

b. Vertical shear

Equation 1 implies that perturbations in horizontal wind in a ducted gravity wave also produce *perturbation vertical shear of the horizontal wind*. For a two-dimensional wave, all horizontal wind perturbations are either in the same direction as wave propagation or in exactly the opposite direction. *So, the perturbation shear is also parallel or anti-parallel to the direction of wave propagation.* Intuitively, based on Fig. 1 and the impedance relationship, the maximum perturbation vertical wind shear ($\partial u'/\partial z > 0$) occurs at the wave trough (where u' is at a minimum at the ground, while $u'=0$ always at the top of the duct). Conversely, the minimum perturbation vertical wind shear ($\partial u'/\partial z < 0$) occurs at the wave ridge. Mathematically, one may derive an expression for the vertical wind shear $\partial u'/\partial z$ in a ducted gravity wave by simply differentiating (1) with respect to z, which produces

$$\frac{\partial u'}{\partial z} = -mB\cos(kx - \omega t)\sin(mz) \qquad (2)$$

Equation 2 shows not only that vertical shear is horizontally 180 degrees out of phase with u', but also that vertical shear is maximized at the top of the duct. Figure 2 shows a plot of the perturbation vertical shear (in the x-z plane) associated with the wave illustrated in Figure 1.

3. Idealized examples

We will first illustrate the effect of a ducted gravity wave on the vertical shear by simulating a ducted wave moving through an idealized environment with a simple background vertical wind shear profile. The ducted wave applied in each case will have similar characteristics to the wave described in section 2a (amplitude 10 m s^{-1}, horizontal wavelength 100 km, and duct depth 2 km). Also in each case, we assume linear westerly shear, with a magnitude of 5 x 10^{-3} s^{-1}, in the background wind profile. Ambient winds are westerly (implying V = 0), and increase from U = 2.5 m s^{-1} at the surface to U = 12.5 m s^{-1} at z = 2 km. A hypothetical storm motion will also be applied, allowing assessment of changes in storm-relative helicity due to the ducted gravity waves.

a. Wave moving in same direction as background shear vector

In this case, the ducted gravity wave is moving parallel to the wind shear vector, or toward the east. Figure 3a illustrates the airflow vectors in the x-z plane for the background wind profile, while figure 3b shows the airflow with the effect of the wind perturbations associated with the ducted wave. Of course, at any given point, the total wind u is the sum of the background wind U and the perturbation wind u'.

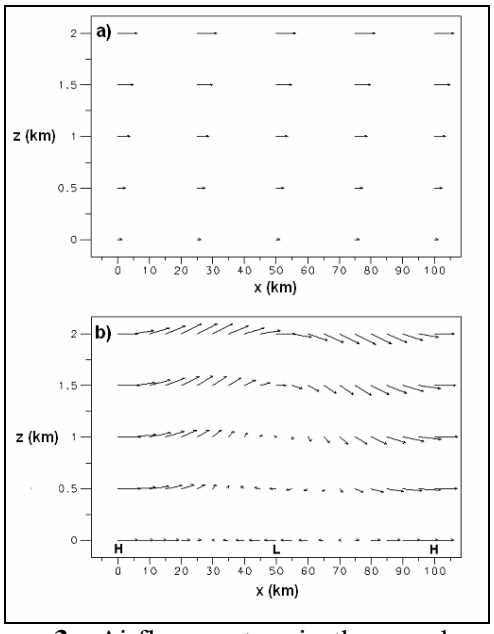

Figure 3. Airflow vectors in the x-z plane for (a) the ambient atmosphere and (b) the atmosphere containing a ducted gravity wave. See text. Notation the same as Figure 1.

Figure 3 illustrates that the introduction of the wave significantly alters the vertical wind shear. For example, at 1.5 km AGL, the magnitude of the vertical shear (initially 5 x 10^{-3} s^{-1}) decreases to -2.3 x 10^{-3} s^{-1} in the wave ridge, and increases to 12.9 x 10^{-3} s^{-1} in the trough, more than double its value outside the influence of the wave. The 0-2 km bulk shear, initially 10 m s^{-1}, decreases to zero in the wave ridge, then

increases to 20 m s^{-1} in the wave trough. If such a wave were propagating at a ground-relative phase speed of 20 m s^{-1}, the change from minimum to maximum shear would occur in only 2500 seconds (about 42 minutes).

Now, suppose a storm is moving 30 degrees to the right of the mean wind direction, which is consistent with Maddox (1976), at a speed of 12.5 m s^{-1}. Three 0-2 km AGL hodographs (including storm-relative winds) are plotted in Figure 4. In the ambient atmosphere (without any ducted wave), the storm-relative helicity (SRH) is a very slight 63 $m^2 s^{-2}$ (Fig. 4a). In the wave ridge, the winds at 0 and 2 km AGL are both 12.5 m s^{-1}, and since the 0-1 km SRH and the 1-2 km SRH are small and cancel, the 0-2 km SRH = 0 (Fig. 4b). However, in the wave trough, the negative low-level wind perturbations have significantly lengthened the hodograph in the direction of wave motion, and SRH = 126 $m^2 s^{-2}$ (Fig. 4c).

b. Wave moving at 45 degree angle to background shear vector

The case described in section 3a is repeated, using the same ambient wind profile and wave amplitude. But, in this case, the wave is moving toward the northeast (from 225 degrees). The SRH is still 64 $m^2 s^{-2}$ in the ambient atmosphere, decreases to 46 $m^2 s^{-2}$ in the wave ridge, and increases to 83 $m^2 s^{-2}$ in the wave trough. Bulk shear is 10 m s^{-1}, 8 m s^{-1}, and 19 m s^{-1} in the ambient atmosphere, ridge, and trough respectively.

The preceding examples demonstrate the significant changes in vertical wind shear and storm-relative helicity associated with only a moderate-amplitude ducted gravity wave. They also illustrate that the angle of the wave motion, relative to the shear vector, plays a role in determining the magnitude of change in bulk shear and SRH.

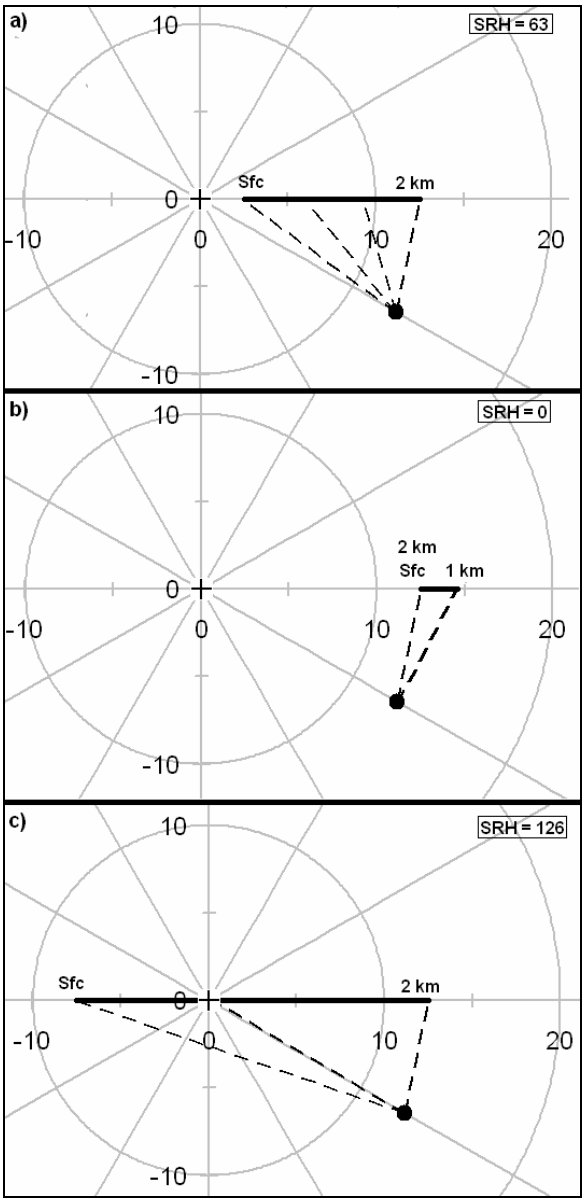

Figure 4. 0-2 km AGL hodographs for the ducted wave case described in section 3a. a) represents the ambient atmosphere, b) represents the wave ridge, and c) the wave trough. The hodograph is marked with speed rings at increments of 10 m s^{-1}, and directional spokes at increments of 30 degrees. SRH is given in $m^2 s^{-2}$.

The natural tendency is for a ducted gravity wave to move with a large component parallel to the mean wind and the bulk shear vector, since the ground-relative motion is simply the vector sum of the intrinsic velocity and the average background wind in the ducting layer. So, the cases in sections 3a and 3b are probably representative of most real situations, with shear increasing in the wave trough and decreasing in the wave ridge. This becomes more significant when one considers that a large percentage of observed large-amplitude ducted gravity waves are waves of depression (e.g., Uccellini and Koch 1987), ie., they consist of a wave trough only.

However, if a wave was moving in a direction with a component opposite the low-level shear vector, the wave-normal shear in the atmosphere would decrease in the wave trough and increase in the wave ridge. Also, since storms typically move to the right of the mean wind, storm-relative helicity may also decrease in the wave trough if a wave is moving against the low-level shear vector, a case in which the wave would typically approach a storm from its left flank.

4. Case Studies

In each of the three cases described in the following subsections, the passage of an apparent ducted gravity wave had a significant impact on the vertical wind shear and the storm-relative helicity.

a. 1 December2006

1) ENVIRONMENT

On the night of 30 November-1 December 2006, a major winter storm occurred in Missouri, with frozen and/or freezing precipitation falling over a large area. The thermodynamic environment was supportive of ducted gravity waves. The 06 UTC NAM sounding at St. Louis (Figure 5a) shows a deep inversion layer from just above the surface up to 725 hPa, with much less stable air above that. This rapid decrease in stability provided an excellent wave reflecting layer, so a wave duct (e.g., Lindzen and Tung 1976; Nappo 2002) was present.

The upper-air pattern was also conducive to gravity wave generation on 2 Feb 2006. In a review of mesoscale gravity wave cases, Uccellini and Koch (1987) found a consistent upper-air pattern favorable for the development of mesoscale gravity waves. These findings were also addressed by Koch and O'Handley (1997). These authors found that gravity waves often occur in the diffluent flow between the 300 hPa inflection axis to the southwest and the 300 hPa ridge axis to the northeast.

The NCEP/NCAR reanalysis 300 hPa geopotential height chart at 00 UTC on 1 Dec 2006 (Figure 5b) shows a deep upper- level trough over the Plains States. The inflection axis in the height contours on the east side of the trough extended from southwest Missouri into northwest Mississippi, with the ridge axis from Iowa into Illinois, *placing most of Missouri in a region favorable for wave generation.*

2) OBSERVATIONS

The ducted wave being examined was evident in surface observations at least as early as 0100 UTC in Arkansas, and moved north-northeastward through eastern Missouri during the evening. The wave was associated with surface pressure oscillations of amplitude 3 to 4 hPa and surface wind perturbations of 5 to 10 m s^{-1} (see Figure 6). The wave ridge was also associated with a band of enhanced reflectivity on radar, and the wave troughs (one ahead of the ridge, one behind the ridge) were associated with bands of decreased reflectivity, consistent with rising motion ahead of the ridge and subsidence ahead of the trough (Figure 7).

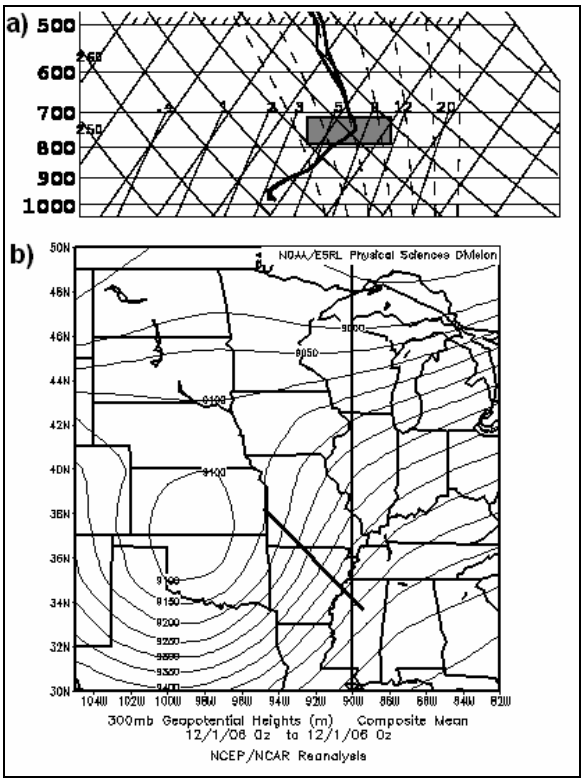

Figure 5. a) Skew-T, ln-p diagram of NAM model sounding at St. Louis, Missouri, 0600 UTC 1 Dec 2006. Gray-shaded area represents top of ducting layer. b) 300 hPa geopotential height (in meters), at 00 UTC, 1 Dec 2006. (NCEP/NCAR Reanalysis). Bold line segment indicates approximate location of inflection axis in height contours.

3) SHEAR

The low-level wind perturbations associated with this gravity wave produced rapid, large changes in vertical shear and helicity. The VAD wind profiles at the LSX WSR-88D (near St. Louis) illustrate these shear changes (Figure 8a). It should be noted that VAD wind analysis is a low-pass filter, and probably smoothes values of *u*' somewhat. A*s* discussed in section 2b, perturbation vertical shear (in the direction of wave motion) is positive in the wave trough, and negative in the wave ridge. The wind profiles in Figure 8a show the low-level wind perturbations associated with northward-moving wave as the lowest level winds veer from northeasterly to southeasterly in less than 30 minutes as the wave ridge passes the radar around 0600 UTC. During the wave trough passage around 0630 UTC, the low-level winds backed quickly to north-northeasterly, in response to negative perturbation winds in the trough.

Figure 8b, the wave-normal 0-3 km AGL wind shear (derived from VAD wind profiles at LSX), indicates the negative perturbation shear in the wave ridge at 0600 UTC, followed quickly by positive perturbation shear in the trough at 0615. The shear increases from 21.7 m s^{-1} in the wave ridge to near 38.9 m s^{-1} in the wave trough, over a time period of less than one hour.

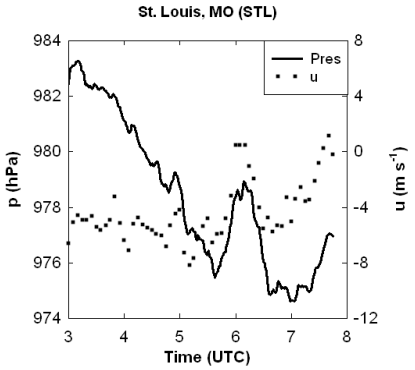

Figure 6. Surface observations of pressure (hPa) and wave-normal wind speed (from azimuth 190 degrees, in m s^{-1}) at St. Louis, MO on 1 Dec 2006. Wave ridge passes station just after 0600 UTC, with trough near 0630 UTC. Note positive perturbation winds associated with the wave ridge.

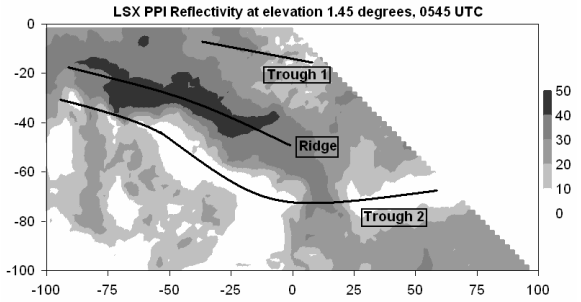

Figure 7. PPI scan of reflectivity (dBZ) at 1.45 degrees elevation from LSX WSR-88D at 0545 UTC, 1 Dec 2006. Rough locations of wave troughs and ridges indicated by reflectivity minima and maxima are shown with bold curves. Axes are labeled in km, with the radar at the origin.

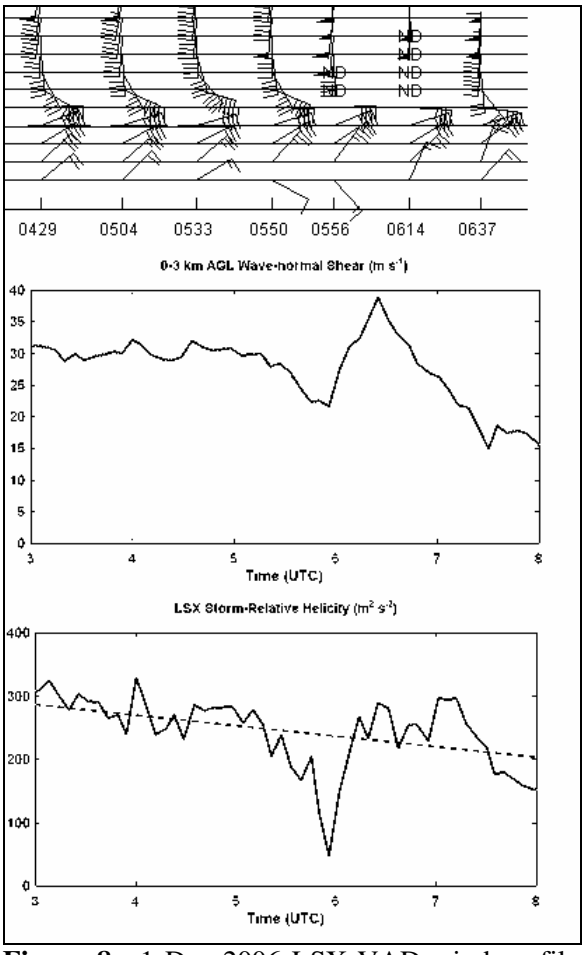

Figure 8. 1 Dec 2006 LSX VAD wind profile a) output at selected times; b) 0-3 km wave-normal wind shear (m s^{-1}); and c) storm-relative helicity (m^2 s^{-2}), with overall linear trend in storm-relative helicity indicated by dashed line (see text.)

This is not a severe storm environment. However, part of the purpose of this paper is to demonstrate that storm-relative helicity in a severe storm environment reacts to ducted gravity waves. Since calculations of the kinematic properties (shear and helicity) of the wind profiles are essentially the same, this environment is still indicative of the shear changes in a storm environment. Using the relatively undisturbed background winds at 0429 UTC, it was determined that the storm motion (75% of the mean 0-9 km AGL wind speed, and 30 degrees to the right, e.g., Maddox 1976) would be from 207 degrees at 15.75 m s^{-1}. This storm motion was applied to VAD wind profiles from the KLSX WSR-88D, allowing for computation of 0-1 km AGL storm-relative helicity (Figure 8c).

Consistent with the idealized examples presented in section 3, the ducted gravity wave caused rapid changes. The storm-relative helicity (SRH) plummeted from 238 m^2 s^{-2} to only 48 m^2 s^{-2} in the wave ridge, a drop of nearly 80% in less than 30 minutes. Then, as the wave trough moved near the radar, the SRH increased back to 289 m^2 s^{-2} by 0625 UTC. This represents a positive perturbation in storm-relative helicity, since background storm relative helicity was decreasing at an average rate of about 17 m^2 $s^{-2}hr^{-1}$ as the surface and 850 hPa lows lifted out farther to the north and east during the evening. This linear trend is indicated in Figure 8c.

b. 2 February 2006

1) ENVIRONMENT

The environment on the morning of 2 February 2006 was supportive of the generation and maintenance of gravity waves over the state of Alabama. A large area of rain, with embedded convection, moved northeast into Alabama out of Mississippi during the early morning hours.

The best estimate of the thermodynamic profile, provided by the 1200 UTC sounding at BMX (Figure 9a), *shows a wave duct between the surface and 2 km AGL.* A stable layer extends to about 2 km AGL, with an abrupt change to a conditionally unstable lapse rate above 2 km AGL, providing the necessary wave reflection.

The upper-air pattern was also conducive to gravity wave generation on 2 Feb 2006. The NCEP/NCAR reanalysis 300 hPa geopotential height chart at 12 UTC on 2 Feb 2006 (Figure 9b) shows a negatively-tilted trough extending from eastern Texas into the northwestern Gulf of Mexico, with a ridge axis from western Kentucky to Georgia. Mississippi and Alabama are within the diffluent flow region between the inflection axis in the height contours and the 300 hPa ridge, *the region favorable for wave generation.*

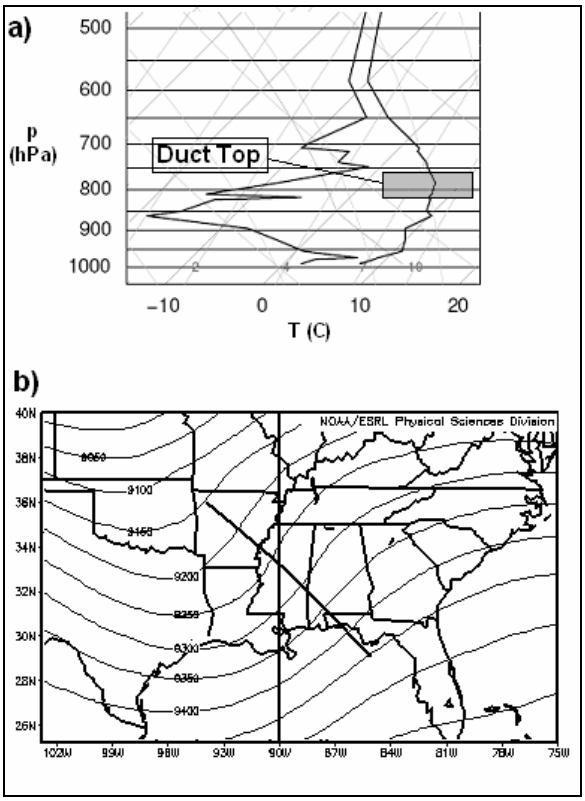

Figure 9. a) Skew-T, ln-p diagram of sounding data from Birmingham, AL (BMX) at 1200 UTC 2 Feb 2006. Gray-shaded area represents top of ducting layer. b) 300 hPa geopotential height (in meters), at 1200 UTC, 2 Feb 2006. (NCEP/NCAR Reanalysis). Bold curve indicates approximate location of inflection axis in height contours.

2) OBSERVATIONS

The ducted wave being examined was evident in surface observations as early as 1050 UTC at Jackson, MS, where a pressure fall of approximately 7 hPa occurred in 30 minutes, accompanied by a wind gust of 13.3 m s^{-1}. The pressure fall/rise couplet continued to move northeastward fairly rapidly (~22 m s^{-1}) through eastern Mississippi and western Alabama through about 1500 UTC. Observations of mean sea level pressure from selected stations in this region are shown in Figure 10.

The wave trough was located very near the back edge of the precipitation area. The large horizontal reflectivity gradient there may be indicative of the subsidence ahead of the wave trough. A PPI scan of radar reflectivity from the WSR-88D at Columbus, MS (KGWX) at 1333 UTC is shown in Figure 11a. The horizontal wind perturbations are maximized at low-levels, as shown in a cross-section of wind perturbation *u*', normal to the direction of wave propagation (Figure 11b). Wind perturbations were derived directly from the base velocity from KGWX at 1333 UTC and the ambient wind profile, assumed to be represented by the VAD wind profile from the KGWX radar at 1159 UTC, well ahead of the wave.

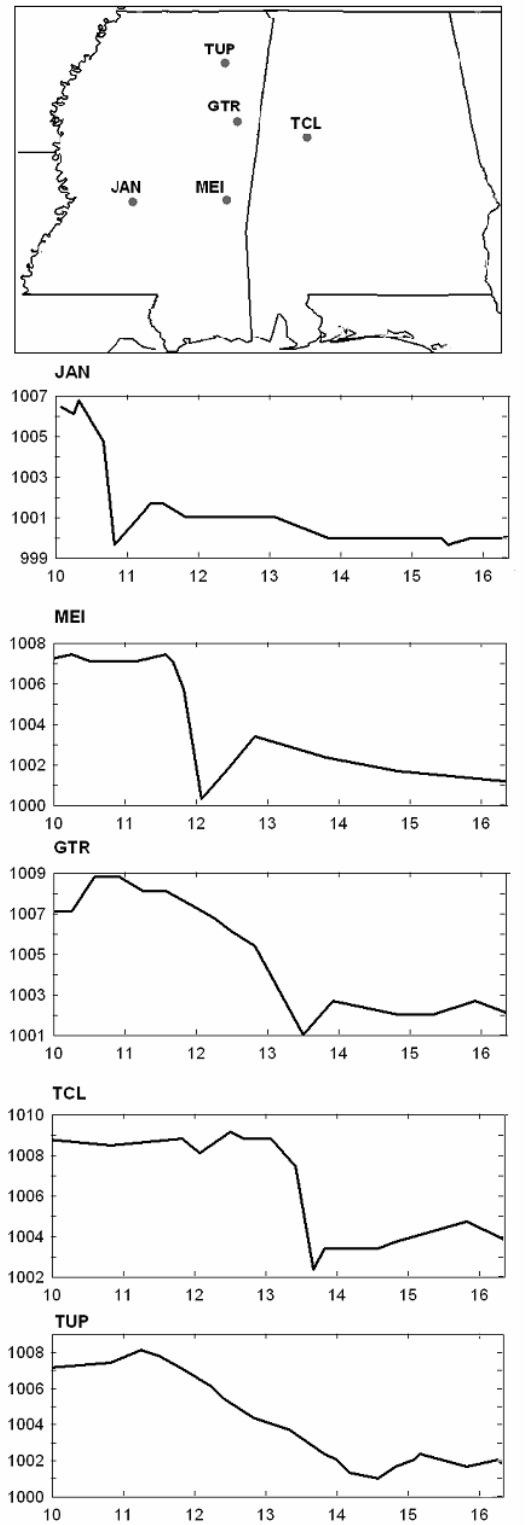

Figure 10. MSL pressure observations on 2 Feb 2006 and map showing observation locations. Times are in UTC, and pressures are in hPa, adjusted to mean sea level. Observations are generally hourly, with some sub-hourly.

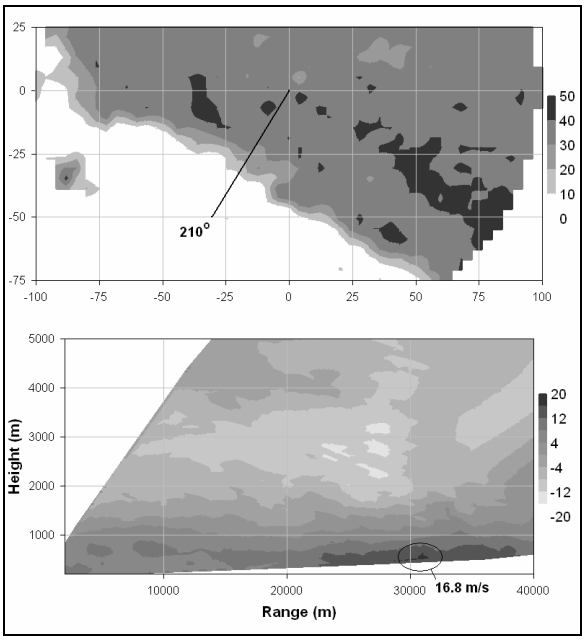

Figure 11. 1333 UTC 2 Feb 2006 KGWX WSR-88D a) PPI scan of reflectivity (in dBZ) at 0.5 degrees (grid is in km, radar at origin), and b) cross-section of u' (in m s^{-1}) along azimuth 210 degrees. Maximum outbound (northeasterly) wind perturbation noted.

The authors acknowledge the *possibility* that the pressure and wind perturbations on 2 February 2006 may be related, at least in part, to a "wake low" phenomenon (e.g., Johnson 2001). However, the portion of the system being examined near the KGWX radar does not have the appearance of a classic squall-line, which is typically associated with a wake low. Further, Haertel and Johnson (2001) point out that a wake low is "more aptly described as a gravity wave phenomenon". Finally, the sinusoidal pattern of wind and pressure at the surface, as well as the wind perturbations being maximized at low-levels, is kinematically similar to that observed in ducted gravity waves, making the distinction in this case somewhat academic.

3) SHEAR

The ducted wave on 2 February 2006 was associated with significant low-level wind perturbations. Since the pressure trough was more significant than the pressure ridge at the surface, the largest wind perturbations were in the opposite direction of wave motion, ie., out of the northeast (from about 030 degrees). The

ambient wind profile well ahead of the wave (1159 UTC) showed primarily southerly winds from the surface through 3 km, with some speed shear (see Figure 12a). The wave trough passed the radar just after 1400 UTC (the GWX radar site is about 50 km northeast of surface station GTR). As it did, low-level winds backed sharply in response to the negative wind perturbations associated with the wave trough. Winds just above the surface changed from 175 degrees/9 m s^{-1} at 1159 UTC, to 100 degrees/14 m s^{-1} at 1407 UTC! Applying the "30R75" method (see section 4a3) to the ambient wind profile to determine a storm motion, 0-3 km AGL storm-relative helicity was

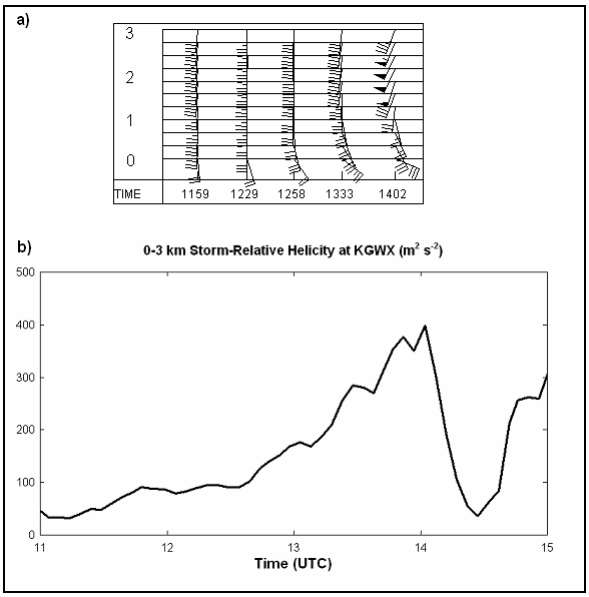

Figure 12. a) VAD wind profiles from KGWX WSR-88D on 2 Feb 2006 (heights in km), and b) 0-3 km AGL storm-relative helicity at KGWX. Note the backing of low-level winds and rapid increase in storm-relative helicity as wave trough passes radar around 1407 UTC.

calculated at each volume scan time at KGWX (Figure 12b). Note that between 1100 and 1300 UTC, storm-relative helicity had been only slowly increasing, from 50 to 150 m^2 s^{-2}, then rapidly increased to near 400 m^2 s^{-2} when the wave trough passed just after 1400 UTC. Storm-relative helicity then decreased rapidly immediately behind the wave trough. In this case*, the passage of the ducted gravity wave caused the storm-relative helicity to double in less than one hour.*

c. 22 January 1999

An outbreak of severe storms occurred over parts of northwest Alabama on 22 January 1999 (*Storm Data, NWS).* However, the environment was also favorable for ducted gravity waves, with a sudden decrease in static stability with height near 2 km AGL. Analysis of the 1800 UTC sounding from Birmingham, Alabama (Figure 13) indicates that this environment would support ducted gravity waves moving northward around 38 m s^{-1}.

Just after 2000 UTC, as intense convective storms were moving into northwest Alabama, two fine lines appeared in radar reflectivity imagery to the southwest of Birmingham. These fine lines, separated by about 40 km, were moving northward at 34 m s^{-1}, very close to the predicted gravity wave speed. Given their speed, and the synoptic-scale environment which was favorable for waves (the 300 hPa mass field as well as large vertical wind shear at low levels), these fine lines were determined to indicate the ridges of ducted gravity waves (for details and radar imagery, see Coleman and Knupp 2007, submitted).

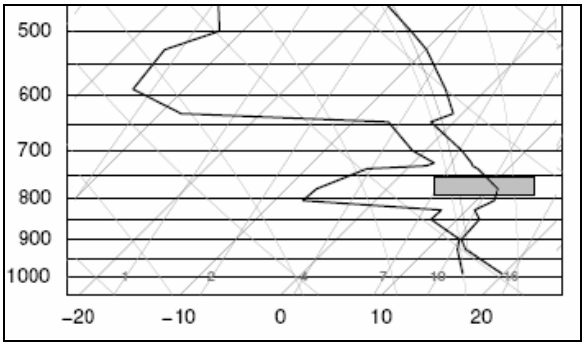

Figure 13. Skew-T, ln-p diagram at Birmingham, AL (BMX) at 1800 UTC on 22 January 1999. Ducting region near 2 km AGL is highlighted.

Ducted waves are to a first approximation two-dimensional; these waves were quasi-steady over a period of time; and both waves passed to the west of the Birmingham, AL WSR-88D radar (BMX). This allowed a form of synthetic dual-Doppler synthesis (e.g., Klimowski and Maurwitz 1992) to be performed in order to determine the wind perturbations within each wave. For example, radial velocities near 1 km AGL in the second wave were measured using Doppler radar data from BMX at azimuth 243° (at 2021 UTC) and at azimuth 297° (at 2052 UTC). Two equations (relating u and v to azimuth and radial velocity) and two unknowns (u and v), enabled computation of u and v within the wave. A similar analysis was also completed for the first wave. Subtracting the wave-normal background wind from computed wind provided the wind perturbation at 1 km AGL. Then, the vertical profiles of horizontal wind perturbations were determined within both waves using equation 1. It was determined that the first wave (northernmost wave) had a maximum u' of 4.4 m s^{-1}, while the second wave was more intense, with maximum u'=14.3 m s^{-1}.

The two-dimensional u' profile, as it changed with time as the waves passed by a point, was combined with the ambient wind profile in the 0-2 km AGL layer, given by the 2011 UTC VAD wind profile from the KBMX radar. This provided an estimate of the time evolution of the wind profile due to the effects of the waves. The wave speed and wavelength provide a wave period of 1176 seconds. In Figure 14, the surface wind perturbation (which, through the wave impedance relation, is proportional to the surface pressure perturbation) is plotted as a function of time through 2 wave periods, beginning ¼ of a wavelength ahead of the ridge associated with the first wave. Along with this plot, the 0-2 km AGL storm-relative helicity (using the observed storm motion from 240 degrees at 20 m s^{-1}), and a time-height section of the wave-normal wind component are included. Note that, as expected for a wave moving with a component in the same direction as the background wind, storm-relative helicity and shear are maximized in the wave troughs and minimized in the wave ridges. The ambient storm-relative helicity was already very high (over 600 m^2 s^{-2}), varied by roughly +/- 100 m^2 s^{-2} with passage of the first, weaker wave, then exceeded 950 m^2 s^{-2} in the trough of the second, stronger wave. This represents *an increase in storm-relative helicity of more than 300 m^2 s^{-2} in only slightly more than 30 minutes*. Hodographs for the ambient atmosphere and the atmosphere in the trough of the second wave are shown in Figure 15.

It should be noted that these waves subsequently interacted with a mesocyclone, significantly increasing its vorticity, and causing tornadogenesis (Kilduff 2006, personal communication); however there are processes involved in a wave/mesocyclone interaction in addition to the perturbation vertical shear associated with the wave (Coleman and Knupp 2007, submitted).

5. Conclusions

Utilizing a fairly simple mathematical model of the airflow within a ducted gravity wave, one can clearly see the significant perturbation vertical shear associated with the wave (Figure 1). For a typical ducted gravity wave, the perturbation shear is positive within the wave trough and negative within the wave ridge. The perturbation vertical wind shear also typically changes the storm-relative helicity in a severe storm environment affected by a ducted gravity wave.

In idealized simulations, the vertical wind shear was maximized when the ducted wave moved in the same direction as the ambient shear vector. This allowed the wind perturbations in the ducted wave, which are maximized at low-levels, to "lengthen" the 0-2 km hodograph in the wave trough and "shorten" the hodograph in the wave ridge. The change in shear associated with the wave was less significant when the wave moved at an angle to the shear vector. This is consistent with the findings of Coleman and Knupp (2007, submitted), who showed that the change in vorticity in a mesocyclone associated with the tilting of the perturbation horizontal vorticity in a ducted gravity wave was proportional to the sine of the angle that the wave motion vector makes with the storm-inflow vector.

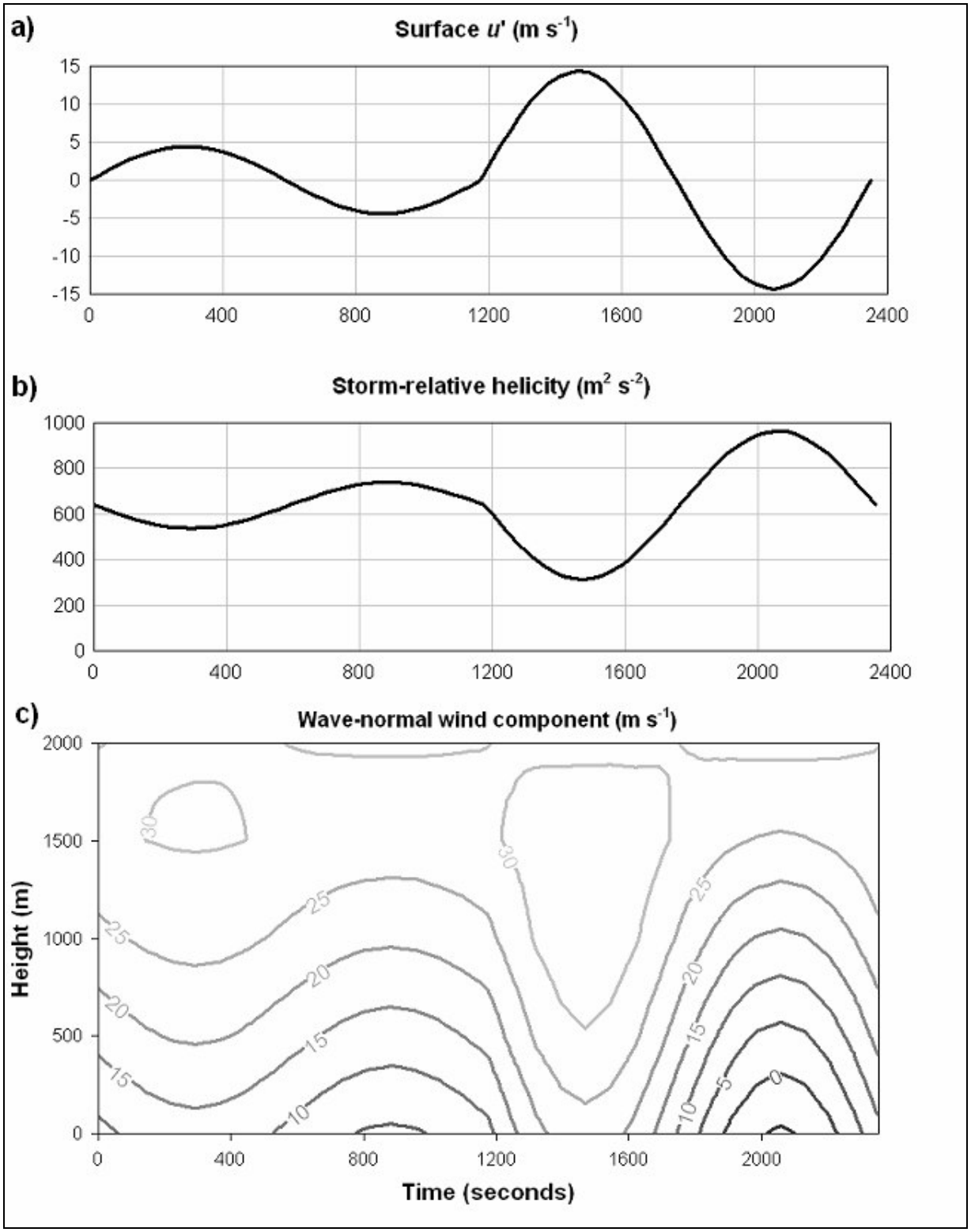

Figure 14. 22 January 1999 synthesized wave-related a) surface wind perturbation (m s^{-1}), b) storm-relative helicity (m^2 s^{-2}), and c) time-height section of wind perturbation (m s^{-1}).

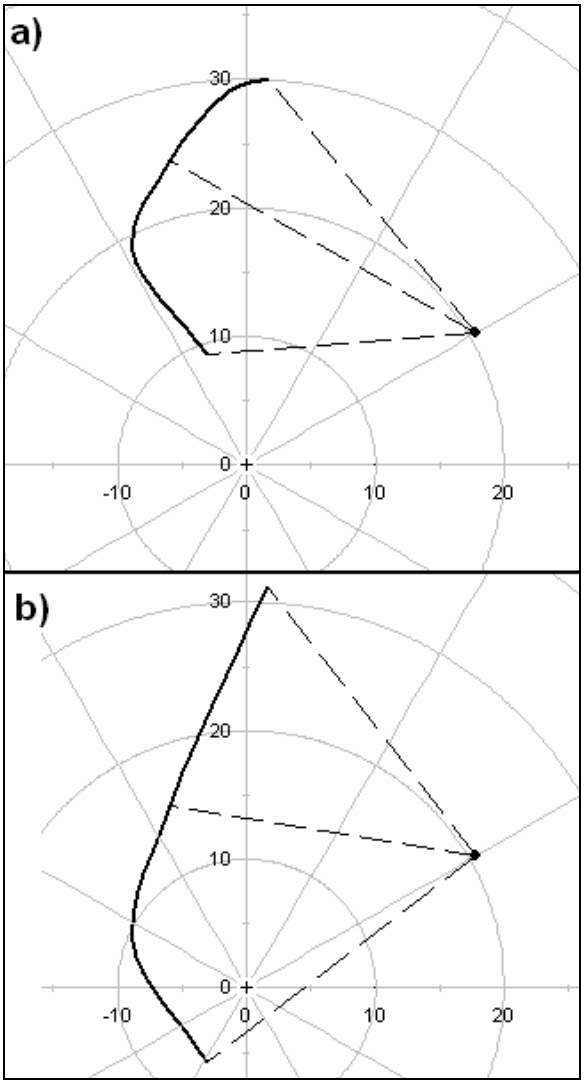

Figure 15. Derived hodographs on 22 January 1999 at a) t=0 (ambient wind profile) and b) t=2059 seconds (in trough of second wave). Wind speed contours are in m s^{-1}, and storm motion is that observed on 22 January 1999.

Three case studies illustrate the effect of a ducted gravity wave on the vertical shear and storm-relative helicity in various environments. In the case of a ducted wave moving through a Missouri winter storm on 1 December 2006, the positive low-level wind perturbations in the wave ridge decreased the wave-normal 0-3 km AGL wind shear, from just over 30 m s^{-1} to about 23 m s^{-1}, then the shear increased rapidly to about 38 m s^{-1} in the wave trough.

The second case study involved a fairly high-amplitude pressure disturbance, apparently a ducted gravity wave, which moved through an environment with fairly linear wind shear. The wave trough produced very large perturbations in low-level winds (16.8 m s^{-1}), and also increased the storm-relative helicity in the environment from near zero to around 400 m^2 s^{-2}. In this case, the wave was moving at an angle to the ambient vertical shear vector. *Even though this may have reduced the net effect on wave-normal vertical shear as discussed above, it caused a sharp backing of the winds at low-levels, which produced a curved hodograph and greatly increased the storm-relative helicity.*

The third case study involved two ducted waves in a severe storm environment which actually went on to interact with and intensify a mesocyclone. Synthetic dual-Doppler analysis, in combination with the idealized two-dimensional perturbation flow structure in a ducted gravity wave and the ambient wind profile, allowed for analysis of the effect of the ducted gravity waves on the helicity in the high-shear environment. Helicity decreased in the second, stronger wave ridge (from over 600 m^2 s^{-2} to less than 400 m^2 s^{-2}), and increased in the wave trough to over 900 m^2 s^{-2}.

It has been shown, through idealized simulations and case studies, that large changes in vertical wind shear and storm-relative helicity may occur on short time scales of O(1 h) within ducted gravity waves. These findings may be further supported by the 12 June 2002 International H_20 project (IHOP; Weckwerth et al. 2004) case presented by Markowski and Richardson (2007), in which gravity waves on the cool side of an outflow boundary may have produced periodic oscillations in 0-1 km SRH, of amplitude 30 m^2 s^{-2}. The typical serial sounding period of 90 minutes used in many previous field studies would not fully resolve the changes we present in this paper. Such rapid changes in vertical shear, in an environment containing severe storms, may cause fluctuations in storm rotation and intensity. A ducted gravity wave with a long wavelength may also enhance the vertical shear sufficiently in some environments to allow initiation of severe

convective storms where none were present earlier. Forecasters must be aware of the potential for ducted gravity waves in a given severe storm environment, and then watch for waves which may rapidly change the rotation in a storm.

Acknowledgements

The authors wish to thank Dr. Carmen Nappo (NOAA, retired), Dr. Steve Koch (NOAA), and Dr. Richard Lindzen (MIT) for their insight on the kinematics of ducted gravity waves. The authors also thank the anonymous reviewers, whose comments significantly improved the manuscript. Funding for this research is provided by grants from the National Science Foundation (ATM-0533596) and the National Oceanic and Atmospheric Administration.

References

Brunk, I. W., 1949: The pressure pulsation of 11 April 1944. *J. Meteor.*, **6**, 181-187.

Bosart, L. F., and F. Sanders, 1986: Mesoscale structure in the Megalopolitan snowstorm of 11-12 February 1983. Part III: A Large amplitude gravity wave. *J. Atmos. Sci.*, **43**, 924-939.

Coleman, T. A., and K. R. Knupp, 2007: The interactions of gravity waves with mesocyclones: preliminary theory and observations. *Mon. Wea. Rev.*, submitted.

Coleman, T. A., and K. R. Knupp, 2006: The interactions of gravity waves with tornadoes and mesocyclones: Theories and observations. *Extended Abstracts, 23rd Conf. on Severe Local Storms*, American Meteorological Society.

Davies-Jones, R., D. Burgess, and M. Foster, 1990: Test of helicity as a tornado forecast parameter. *Preprints - 16th Conf. on Severe Local Storms*, Amer. Meteor. Soc., 588-592.

Eom, J.-K., 1975: Analysis of the internal gravity wave occurrence of 19 April 1970 in the Midwest. *Mon. Wea. Rev.*, **103**, 217-226.

Freeman, J. C., 1948: An analogy between the equatorial easterlies and supersonic gas flows. *J. Meteor.*, **5**, 138-146.

Gossard, E. E., and W. H. Hooke, 1975: Gravity waves in the atmosphere. Elsevier, 475 pp.

Gossard, E. E., and W. Munk, 1954: On gravity waves in the atmosphere. *J. Meteor.*, **11**, 259-269.

Haertel, P. T., and R. H. Johnson, 2000: The linear dynamics of squall line mesohighs and wake Lows. *J. Atmos. Sci.*, **57**, 93-107.

Houze, R. A., 1993: Cloud Dynamics. Aacdemic Press, 573 pp.

Jin, Y., S.E. Koch, Y.-L. Lin, F.M. Ralph and C. Chen. 1996: Numerical simulations of an observed gravity current and gravity waves in an environment characterized by complex stratification and shear. *J. Atmos. Sci.,* **53**, 3570–3588.

Johnson, R. H., 2001: Surface mesohighs and mesolows. *Bull. Amer. Meteor. Soc.*, **82**, 13-31.

Kilduff, R. E., 2006: Personal communication.

Kilduff, R. E., 1999: The interaction of a gravity wave with a thunderstorm. Electronic poster, NOAA/National Weather Service.

Klemp, J. B., 1987: Dynamics of tornadic thunderstorms. *Annu. Rev. Fluid Mech.*, **19**, 369-402.

Klimowski, B. A., and J. D. Marwitz, 1992: The synthetic dual-Doppler analysis technique. *J. Atmos. Ocean. Tech.*, **9**, 728-745.

Koch, S. E., and C. O'handley, 1997: Operational forecasting and detection of mesoscale gravity waves. *Wea. Forecasting*, **12**, 253-281.

Lindzen, R. S., and K. –K. Tung, 1976: Banded convective activity and ducted gravity waves. *Mon. Wea. Rev.*, **104**, 1602-1617.

Maddox, R. A., 1976: An evaluation of tornado proximity wind and stability data. *Mon. Wea. Rev.*, **104**, 133-142.

Markowski, P., and Y. Richardson, 2007: Observations of vertical wind shear heterogeneity in convective boundary layers. *Mon. Wea. Rev.*, **135**, 843-861.

Miller, D. A., and F. Sanders, 1980: Mesoscale conditions for the severe convection of 3 April 1974 in the East-Central United States. *J. Atmos. Sci.,* **37,** 1041-1055.

Nappo, C. J., 2002: An introduction to atmospheric gravity waves. Academic press, 276 pp.

Rotunno, R., and J. B. Klemp, 1985: On the rotation and propagation of simulated supercell thunderstorms. *J. Atmos. Sci.*, **42**, 271-292.

Rotunno, R., and J. B. Klemp, 1982: The influence of the shear-induced pressure gradient on thunderstorm motion. *Mon. Wea. Rev.*, **110**, 136-151.

Scorer, R., 1949: Theory of waves in the lee of mountains. *Quart. J. Roy. Meteor. Soc.,* **75,** 41–56.

Trexler, C. M., and S. E. Koch, 2000: The life cycle of a mesoscale gravity wave as observed by a network of Doppler wind profilers. *Mon. Wea. Rev.*, **128**, 2423-2446.

Uccellini, L. W., and S. E. Koch, 1987: The synoptic setting and possible energy sources for mesoscale wave disturbances. *Mon. Wea. Rev.*, **115**, 721-729.

Weckwerth and Coauthors, 2004: An overview of the International H2O Project (IHOP) and some preliminary highlights. *Bull. Amer. Meteor. Soc.,* **85,** 253–277.

Weisman, M. L., and J. B. Klemp, 1984: The Structure and Classification of Numerically Simulated Convective Storms in Directionally Varying Wind Shears. *Mon. Wea. Rev.*, **112**, 2479-2498.

Weisman, M. L., and J. B. Klemp, 1982: The dependence of numerically simulated convective storms on vertical wind shear and buoyancy. *Mon. Wea. Rev.*, **110**, 504-520.